JACS
JOURNAL OF THE AMERICAN CHEMICAL SOCIETY

ARTICLE

pubs.acs.org/JACS

Metal-Specific Interactions of H_2 Adsorbed within Isostructural Metal−Organic Frameworks

Stephen A. FitzGerald,*[,†] Brian Burkholder,[†] Michael Friedman,[†] Jesse B. Hopkins,[†] Christopher J. Pierce,[†] Jennifer M. Schloss,[†] Benjamin Thompson,[†] and Jesse L. C. Rowsell*[,‡]

[†]Department of Physics and Astronomy, Oberlin College, Oberlin, Ohio 44074, United States

[‡]Department of Chemistry and Biochemistry, Oberlin College, Oberlin, Ohio 44074, United States

Supporting Information

ABSTRACT: Diffuse reflectance infrared (IR) spectroscopy performed over a wide temperature range (35−298 K) is used to study the dynamics of H_2 adsorbed within the isostructural metal−organic frameworks M_2**L** (M = Mg, Mn, Co, Ni and Zn; **L** = 2,5-dioxidobenzene-1,4-dicarboxylate) referred to as MOF-74 and CPO-27. Spectra collected at H_2 concentrations ranging from 0.1 to 3.0 H_2 per metal cation reveal that strongly red-shifted vibrational modes arise from isolated H_2 bound to the available metal coordination site. The red shift of the bands associated with this site correlate with reported isosteric enthalpies of adsorption (at small surface coverage), which in turn depend on the identity of M. In contrast, the bands assigned to H_2 adsorbed at positions >3 Å from the metal site exhibit only minor differences among the five materials. Our results are consistent with previous models based on neutron diffraction data and independent IR studies, but they do not support a recently proposed adsorption mechanism that invokes strong $H_2\cdots H_2$ interactions (Nijem et al. *J. Am. Chem. Soc.* **2010**, *132*, 14834−14848). Room temperature IR spectra comparable to those on which the recently proposed adsorption mechanism was based were only reproduced after contaminating the adsorbent with ambient air. Our interpretation that the uncontaminated spectral features result from stepwise adsorption at discrete framework sites is reinforced by systematic red shifts of adsorbed H_2 isotopologues and consistencies among overtone bands that are well-described by the Buckingham model of molecular interactions in vibrational spectroscopy.

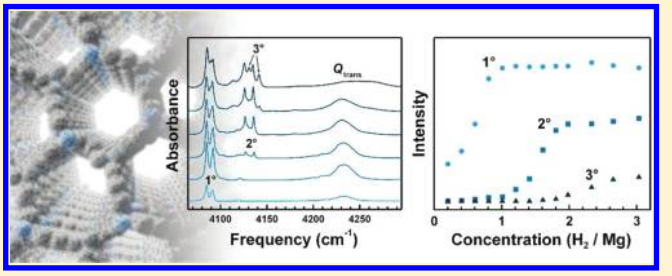

1. INTRODUCTION

It is envisioned by many that supplanting the inveterate combustion engine with modern fuel cell technology employing hydrogen as an energy carrier will greatly decrease our impact on the global environment. Efficient and safe storage of hydrogen is just one of the unsolved puzzles that comprise this enticing, yet formidable goal. Although the past decade of research has yielded an inventory of microporous materials with very large specific surface areas and pore volumes for reversibly containing H_2 molecules,[1−9] the average adsorption enthalpies of these physisorbents fall short of the targeted range of −15 to −25 kJ/mol that is theoretically necessary for operation at room temperature.[10−12] Zeolites and some metal−organic frameworks (MOFs) contain available cation coordination sites to which stronger binding of H_2 has been observed.[14−15] These highly attractive sites typically constitute a small fraction of the surface sites within a given material, obviating their practical use for hydrogen storage. In spite of this, these materials are of great interest as model systems because the quantum dynamics of H_2 in their pores provides critical information for predicting the viability of other known or proposed structures.

The structure type adopted by the material *catena*-(μ_8-2,5-dioxidobenzene-1,4-dicarboxylato)dizinc(II), referred to as MOF-74 and Zn-CPO-27,[17,16] has aroused considerable interest because of its relatively large density of available coordination sites and a respectable micropore volume. This M_2**L** framework (**L** = 2,5-dioxidobenzene-1,4-dicarboxylate) is especially attractive to those investigating the interactions of small molecules in cavities because isostructural materials may be prepared from several metal dications (M = Mg,[18,19] Mn,[20] Fe,[21] Co,[22] Ni,[23] Zn[16]), offering the opportunity to examine site-specific alterations to the adsorption surface. Isostructural series are rare among MOFs, and it has already been shown that the isosteric enthalpy of H_2 adsorption (at small surface coverage) ranges from −8.5 to −13 kJ/mol among the members of the M_2**L** series.[20] These values suggest that microporous adsorbents with average adsorption enthalpies surpassing −15 kJ/mol may be within reach.

Despite several experimental studies and theoretical treatments of the adsorption properties of M_2**L**, uncertainties remain regarding the mechanism by which H_2 binds at different sites and the degree to which H_2 molecules on neighboring sites interact.[14,24] One technique that has proven effective for revealing details of the dynamics of H_2 within porous structures is infrared (IR)

Received: July 29, 2011
Published: November 10, 2011

spectroscopy.[11,24−33] Unperturbed, gaseous H_2 is IR inactive, but upon adsorption weak IR signals arise due to interaction-induced dipole moments. The frequency and relative intensity of these spectral bands provide a measure of the different interaction mechanisms (e.g., inductive, dispersive, and electrostatic) at a particular adsorption site, as well as a means for distinguishing between competing theoretical descriptions of these interactions. In general, MOFs containing available coordination sites exhibit IR spectra with H_2 vibrational bands that are significantly red-shifted compared to frameworks lacking these highly attractive sites.[24] In the case of M_2**L** it has been independently shown that spectra measured at low temperature (and low H_2 concentration[33]) are dominated by these strongly red-shifted bands.[11,24,33] Furthermore, low temperature neutron diffraction studies revealed that adsorbed H_2 first occupies the available metal coordination site, and following saturation of this site other secondary sites become occupied.[34] The conclusion has thus emerged that the IR bands that are most red-shifted are assignable to isolated H_2 at the metal site.

Recently, Chabal and co-workers challenged this conclusion by invoking an unusual H_2 pairing interaction to explain their IR spectra of H_2 in M_2**L**.[35] In this scenario, H_2 at the metal site exhibits a moderate shift in its vibrational frequency, and it is only through interaction with another H_2 at an adjacent secondary site that the IR bands become strongly red-shifted to the value reported by ourselves and others.[11,24,33] In this scenario, $H_2\cdots H_2$ interactions are hypothesized to dominate over differences in the site-specific binding potentials. If this were true the consequences would be profound, both for theoretical modeling, in which $H_2\cdots H_2$ interactions are often neglected, but also (as the authors point out) for the utility of variable-temperature IR spectroscopy in estimating site-specific adsorption enthalpies. Calculations using van der Waals density functional theory (vdW-DFT) were presented to support the authors' claim for such a large frequency shift resulting from $H_2\cdots H_2$ interactions; however, the magnitude of this shift contradicts our previous interpretation of the spectra.[33] Consequently, a definitive experimental analysis is required to test the capability of vdW-DFT to accurately model H_2 adsorption.

Given that the M_2**L** structure type is an important model system for understanding the interactions of H_2 within microporous physisorbents, we have attempted to reproduce the observations of the Chabal group (being particularly mindful of the long equilibration times emphasized in their paper) to scrutinize their proposed H_2 pairing interaction. Through careful sample preparation and handling we have acquired spectra from H_2 in five different M_2**L** materials (M = Mg, Mn, Co, Ni, Zn), all of which are consistent with the original adsorption model developed by ourselves and others. We find that, regardless of temperature or equilibration time, the spectra acquired with the smallest concentrations of adsorbed H_2 display only the strongly red-shifted vibrational bands originally reported.[11,24,33] Moreover, we are only able to reproduce the spectra presented by the Chabal group after deliberately exposing our samples to air, which is known to introduce adsorbed species (particularly water) that tenaciously bond to available metal coordination sites. To complete our study of this system, we have measured the spectra of the adsorbed isotopologues HD and D_2 in these materials and confirmed consistencies among their fundamental and overtone bands that adhere to the well-established Buckingham model of quantized rotational dynamics. We present the results of this study to accelerate the development of accurate models of H_2 adsorption.

2. MATERIALS AND EXPERIMENTAL METHODS

Crystalline samples of M_2**L** (M = Mg, Mn, Co, Ni, and Zn) were prepared using reported procedures with minor modifications.[18,20,36] Reaction solutions were prepared in 100 mL volumes, filtered, and transferred to 250 mL glass bottles sealed with heat-resistant screw caps fitted with Teflon liners. Solvents were thoroughly sparged with nitrogen gas prior to use and during dissolution of the precursors. Reaction vessels were placed in a preheated forced-convection oven (100 °C for M = Co, Ni, Zn; 125 °C for M = Mg, Mn) and removed after 24 h. The solid products were immediately separated by filtration and rinsed with *N*,*N*-dimethylformamide followed by copious amounts of deionized water. Exchange of water for adsorbed species within the pores of the materials was effected by immersing the solids in large volumes (∼100 mL) of deionized water that were decanted and replenished every 12 h over a three day period. The solids were then separated by filtration and transferred to an airtight glass vessel connected to a vacuum manifold. After evacuating for several hours until the samples were free-flowing powders, the vessel was immersed in a silicone oil bath and heated at 2 °C/min to 200 °C and maintained at this temperature for at least 4 h under dynamic vacuum. Samples were agitated periodically to improve temperature homogeneity. After cooling to room temperature, the sealed vessel was transferred to an argon glovebox to recover the dehydrated material.

The composition and crystalline phase purity of each sample was confirmed by a combination of Fourier transform infrared (FTIR) spectroscopy, thermogravimetric analysis (TGA), powder X-ray diffraction (PXRD), and hydrogen gas adsorption measurements. FTIR spectra were measured with 2 to 4 cm^{-1} resolution using a Nicolet 6700 spectrometer equipped with an attenuated total reflectance accessory (Smart iTR, Thermo Scientific). TGA was performed by heating ∼10 mg of sample in an alumina crucible at a constant rate of 2 °C/min under flowing prepurified nitrogen or dry compressed air and monitoring the mass changes (TA Instruments SDT 2960). Powder X-ray diffraction was performed on samples packed into flat plates using Cu Kα radiation with Bragg−Brentano or parallel beam geometries (Rigaku Ultima IV diffractometer). Samples were dehydrated in situ under flowing nitrogen by raising the sample temperature by 2 °C/min to specified set points for data collection using a programmable low/medium temperature attachment (Rigaku). Hydrogen adsorption isotherms were measured at 77 K up to a pressure of 1 atm using a custom-fabricated Sieverts apparatus. Dehydrated samples (∼0.1 g) were loaded in a stainless steel adsorption cell within an argon glovebox and evacuated on the manifold of the apparatus for several hours before analysis. The manifold was flushed with hydrogen multiple times before immersing the adsorption cell in liquid nitrogen and dosing the sample with hydrogen in a stepwise manner. The pressure changes were monitored using a transducer (Omega PX-303), with 15 min observed to be generally sufficient for equilibration of each dosing step.

Infrared spectra were acquired using a Bomem DA3 Michelson interferometer equipped with quartz-halogen and glowbar sources, CaF_2 beamsplitter, and a liquid nitrogen cooled mercury−cadmium−telluride detector. A custom-built diffuse reflectance system with a sample chamber that allows both the temperature and atmosphere of the material to be controlled was utilized for all experiments.[37] Samples of M_2**L** (∼10 mg) were transferred under inert atmosphere to a cup affixed to a copper slab providing thermal contact to a coldfinger cryostat (Janis ST-300T). The sample temperature was monitored by a Si-diode thermometer placed directly within the sample cup. Prior to introduction of the hydrogen gas, the samples were evacuated for several hours at room temperature. Volumes of research grade H_2, HD, and D_2 (99.9999% purity) were dispensed from a calibrated gas manifold. In a typical experiment, a reference spectrum was first obtained of the evacuated material at 35 K. The sample was then heated to 150 K, exposed to a known quantity of

H_2, and cooled slowly to 35 K before acquiring a spectrum. The quantity of H_2 adsorbed was determined by changes in the manifold pressure. Control experiments were also performed with a nonadsorbing sample such as CaF_2 and by exposing M_2**L** samples to He gas.

3. THEORETICAL BACKGROUND

Free H_2 vibrates at an IR inactive frequency of 4161 cm^{-1} and acts as a near-perfect quantum rotor with rotational energy levels $E_J = B_v J(J + 1)$, where J is the rotational quantum number and B_v is the rotational constant for a given vibrational state v.[38] As a result of quantum statistics, the H_2 molecule exists as either *ortho*-H_2 with total nuclear spin $I = 1$ and odd J quantum numbers or as *para*-H_2 with $I = 0$ and even J. These restrictions fundamentally limit all photon-induced transitions to $\Delta J = 0$ (Q transitions) or $\Delta J = \pm 2$ (S and O transitions).[39] In the absence of *ortho* to *para* conversion there are four possible transitions at low temperature: purely vibrational $Q(0)$ and $Q(1)$, which differ by only 6 cm^{-1} in the gas phase, and the rovibrational transitions $S(0)$ and $S(1)$ (numbers in parentheses indicate the initial rotational state). The interaction of H_2 with surface atoms modifies both the vibrational and rotational constants and lifts the $2J + 1$ degeneracy of the rotational levels. This leads to frequency shifts, splittings, intensity changes, and activation of IR absorption bands, all of which are correlated with the symmetry and the interaction energy of the binding site. Adsorbed H_2 can also undergo translational transitions in which it changes its center-of-mass quantum state. Bands associated with these translational transitions tend to be broader than those arising from pure rovibrational transitions.[29,40,41]

There are two basic mechanisms by which interaction-induced dipole moments can lead to IR activity. In the first mechanism, framework atoms interact with the H_2 polarizability to induce a dipole moment on the molecule. The H_2 polarizability is essentially isotropic, and so to a good approximation this mechanism only activates Q transitions.[42] Herein, we refer to this as the *isotropic mechanism*. The second mechanism involves the quadrupole moment of H_2 inducing a dipole moment on the framework atoms, and is denoted the *quadrupole-induction mechanism*. The quadrupole moment of H_2 is highly anisotropic, and this term leads to activation of rovibrational $S(0)$, $S(1)$, and purely vibrational $Q(1)$ transitions. In contrast, $Q(0)$ transitions are not activated because the $J = 0$ state is spherically symmetric and possesses no quadrupole moment in the initial and final states.[43]

4. RESULTS AND DISCUSSION

Sample Preparation and Characterization. Samples of the isostructural materials were prepared by solvothermal reaction of a soluble metal(II) precursor with the protonated form of the structural ligand. Differences in the solvent composition (which includes *N*,*N*-dimethylformamide, ethanol, and water) and reaction temperature were used to improve product yield and crystal quality, as described in the literature.[18,20,36] It was observed that thoroughly sparging the solutions with nitrogen gas prior to heating minimized solvent oxidation, which is evident by brown discoloration of the product mixtures, particularly in reactions containing nickel(II) and cobalt(II). It is hypothesized that oxidative solvent degradation yields byproducts that are strongly adsorbed within the framework pores and the formation of these byproducts should be prevented. To facilitate desolvation of the pores, samples were immersed in water, which extracts and replaces initially adsorbed species.

Results of PXRD and TGA of the hydrated materials were in good agreement with those reported by the Dietzel group,[17,19,23] who employed water and tetrahydrofuran as the reaction solvents. Variable temperature PXRD revealed the expected changes in the relative intensities of reflections during the desolvation process, below 150 °C. Between 150 and 300 °C there were negligible changes in the diffraction patterns of each material, indicating the samples were solvent-free and their crystallinity was maintained. Comparison of the patterns of the five samples with each other (see Figure S1) and with calculated patterns of the desolvated structures confirmed the phase purity of the crystalline fractions. The thermal behavior observed by PXRD was consistent with observations by TGA, which indicated that desolvation of the samples was complete by 180 °C, as shown in Figures S2−S6. Together with results from previous reports, these observations lead us to choose 200 °C as the desolvation temperature for the bulk samples. In some previous reports methanol has been used as the exchange solvent for the M_2**L** structure type, yet we found that exchange with water was just as effective for producing high-quality samples, in agreement with the observations of the Dietzel group.

The compositional purity of the samples was checked by TGA under flowing air. Oxidation of the organic ligand leaves the corresponding metal oxide (MgO, Mn_3O_4, Co_3O_4, NiO, or ZnO) as residue, and the observed mass changes were in good agreement with calculated values (see Figures S2−S6). For Mn_2**L**, Co_2**L**, and Ni_2**L** the oxidation step was observed to begin around 200 °C; while these materials have confirmed stabilities above this temperature under inert atmospheres, it is noted that small partial pressures of oxygen present while heating above 200 °C will likely cause sample degradation.

Desolvated samples were further characterized by FTIR and H_2 adsorption measurements. Small aliquots of the materials were examined using attenuated total reflectance by compressing the powder on the surface of a ZnSe crystal. IR spectra collected within 60 s after exposing a sample to ambient air display bands characteristic of the structure type (see Figure S7 and Table S1) and no bands corresponding to water or residual solvent in the pores. Within minutes, however, the absorbance features of water became readily apparent (see Figure S8). Monitoring the rate of rehydration was improved by releasing the anvil compressing the sample, stirring the powder to homogenize exposed grains, and repressing the sample before collecting the next spectrum. Our observations reinforce recommendations that desolvated MOF samples should be stored and handled under an inert atmosphere to ensure optimal performance. We have confirmed the requisite porosity of our samples by measuring their adsorption of H_2 at 77 K up to a pressure of 1 atm (see Figure S9).

Adsorbed H_2 IR Band Assignments. Figure 1 compares representative spectra for H_2 loaded in M_2**L** at 35 K and acquired at 35 K, the lowest temperature examined in this study. For each material, spectra are shown for both a small H_2 concentration (~1 H_2/M) and a large concentration (>2 H_2/M). Each spectrum can be divided into three regions: (1) the Q-band region arising from purely vibrational motion of the adsorbed H_2 and occurring between 4000 and 4150 cm^{-1}, (2) the region from 4150 to 4300 cm^{-1} associated with changes in the center-of-mass translational quantum number, and (3) the S-band region from 4250 to 4700 cm^{-1}, where one observes rovibrational bands.

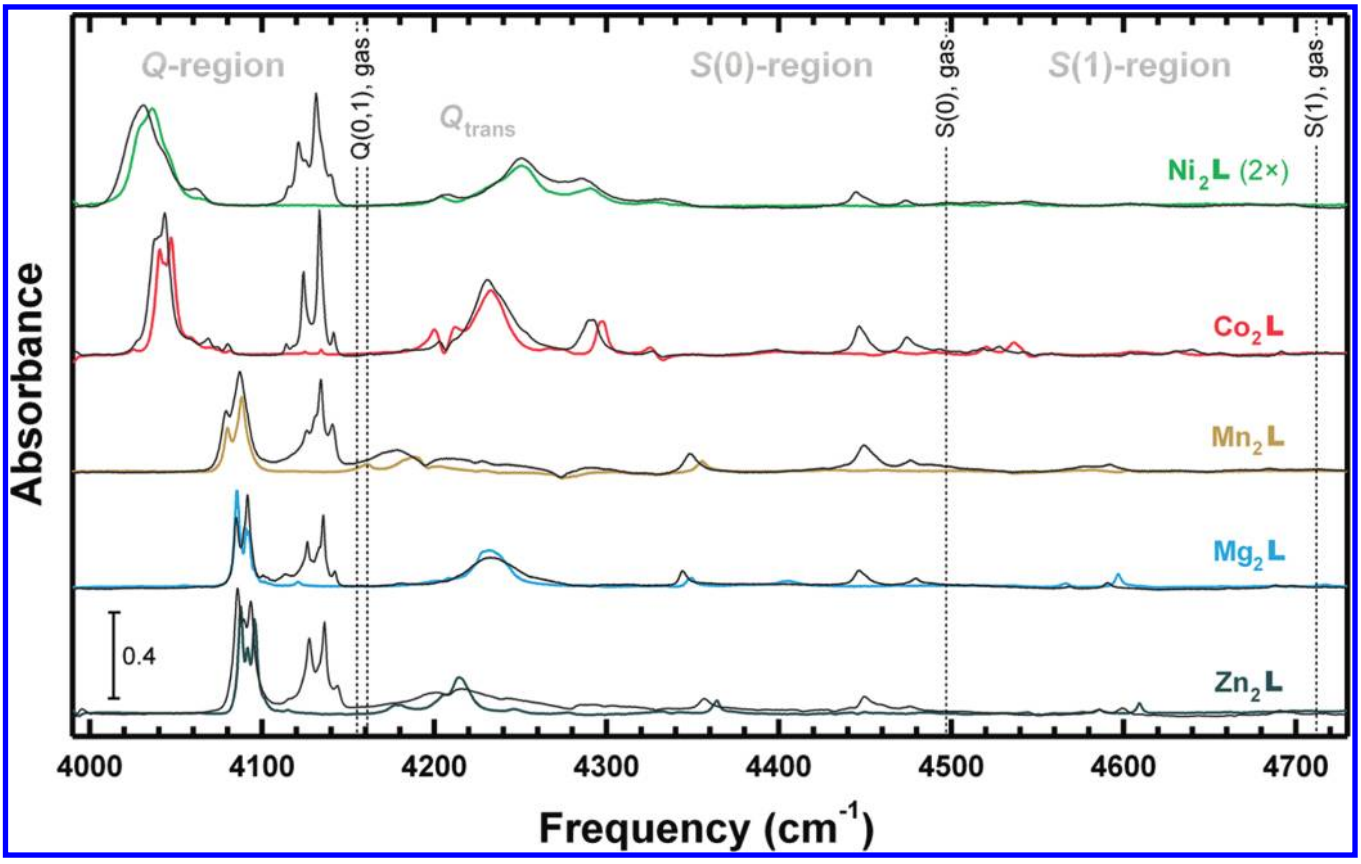

Figure 1. Diffuse reflectance IR spectra of adsorbed H_2 in isostructural M_2**L** frameworks at 35 K. Light-colored traces correspond to adsorbed H_2 concentrations less than 1 H_2/M, and dark gray traces correspond to >2 H_2/M. Spectra are offset for clarity and have a resolution of 1 cm^{-1}. The spectra of H_2 in Ni_2**L** have been magnified by a factor of 2 for comparison.

In all cases the *Q*-bands are more intense than the *S*-bands, indicating that the isotropic mechanism is dominant over the quadrupole-induction mechanism. Similar intensity relationships have been observed for H_2 in other MOFs and zeolites.[25,30,31] In contrast, H_2 in C_{60} gives *S*-bands of comparable intensity to the *Q*-bands, which was attributed to the large polarizability of the C_{60} molecules.[29,41] As expected for low temperature spectra, the translational sidebands associated with *Q*-transitions are observed on the high frequency side of the *Q*-bands, and these are broader than the parent *Q*-bands. The translational sidebands are most likely composed of multiple overlapping bands, reflecting the asymmetry of the adsorption sites. We did not detect translational sidebands associated with the *S*-transitions, probably due to their smaller intensities.

The spectra acquired with smaller H_2 concentrations (light-colored spectra in Figure 1) exhibit notable differences among the five materials, particularly in the *Q*-region between 4000 and 4100 cm^{-1}. In contrast, the secondary bands that emerge after more H_2 is adsorbed (dark gray spectra in Figure.1) appear at similar frequencies and with similar relative intensities for each material. These include new *Q*-bands between 4110 and 4150 cm^{-1} and *S*-bands between 4440 and 4500 cm^{-1}. To explore the concentration dependence of the spectral features in more detail, we performed experiments in which the system was loaded with a known quantity of H_2 at 150 K, and then cooled slowly to 35 K. It has been suggested that a few hours may be required for such a system to attain thermal equilibrium;[35] however, we observed no significant differences between spectra acquired after temperature ramps lasting 30 min or 3 h. Representative spectra for Mg_2**L** are presented in Figure 2. At the smallest concentration, the only bands are an *ortho*/*para* pair in the region 4080−4100 cm^{-1}. The assignment of these to an *ortho*/*para* pair was confirmed previously using *para*-enriched H_2 in Zn_2**L**.[33] The integrated intensity of these bands increases with H_2 concentration until saturating at a concentration of 1.0 H_2/M. At this concentration a second *ortho*/*para* pair appears at 4127 and 4136 cm^{-1}, and the intensity of these bands similarly increases with concentration until saturation at 2.0 H_2/M. The pattern is repeated by a third pair of bands at 4131 and 4141 cm^{-1} for concentrations between 2.0 and 3.0 H_2/M.

While other researchers have presented IR spectra of H_2 in MOFs as a function of loading pressure,[11,24,35] none have analyzed these data stoichiometrically in terms of the number of adsorbed H_2 per metal ion. Doing so allows us to directly compare our spectra with reported neutron diffraction models.[34] These indicated that at 4 K an adsorbed D_2 molecule (an isotopologue of H_2) first occupies the available coordination site of the metal ion, with its center-of-mass 2.6 Å from the metal. This is the only site reportedly occupied up to a loading of 1.0 D_2/M. Above this concentration, the occupancy of this primary site remains essentially complete, while a second site located above a triangle of oxygen atoms begins to fill. Similarly, a third site close to the benzene ring becomes occupied for loadings greater than 2 D_2/M. On the basis of these results, it can be stated with confidence that the IR *ortho*/*para* pair centered at 4090 cm^{-1} is associated with the metal site, while the

dx.doi.org/10.1021/ja2071384 |*J. Am. Chem. Soc.* 2011, 133, 20310–20318

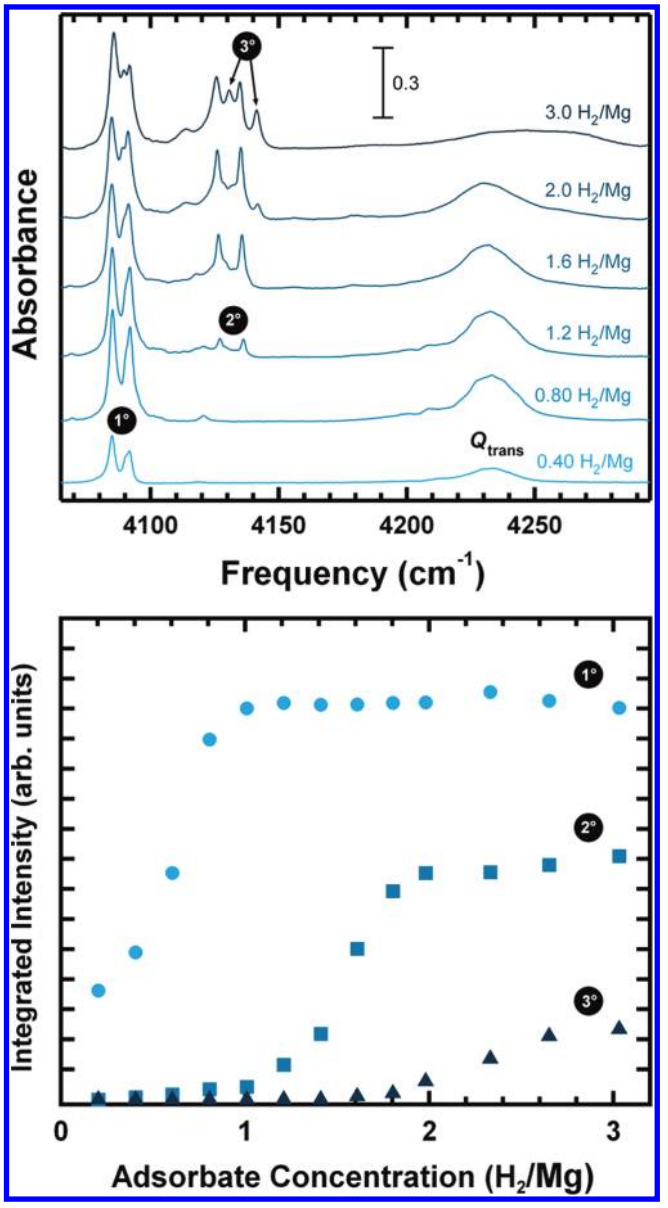

Figure 2. Upper plot: IR spectra demonstrating the concentration dependencies of *Q*-bands in the spectra of H_2 in Mg_2**L** at 35 K. The appearance of bands assigned to H_2 adsorbed at the primary (1°), secondary (2°), and tertiary (3°) sites are noted. The translational sideband of the primary transition is labeled Q_{trans}. Spectra are offset for clarity and have a resolution of 1 cm^{-1}. Lower plot: the deconvoluted, integrated intensities of the primary (●), secondary (■), and tertiary (▲) *ortho*/*para* paired bands with increasing adsorbate concentration, determined by parallel manometry measurements.

bands in the region 4125−4145 cm^{-1} arise from H_2 adsorbed at the oxygen and benzene sites.

In the alternative scheme for the adsorption process proposed by Chabal and co-workers,[35] the isolated occupancy of the metal site produces initial bands around 4125 cm^{-1}, and only after occupancy of secondary sites do these bands shift to the 4090 cm^{-1} region, due to appreciable $H_2\cdots H_2$ interactions. This interpretation is irreconcilable with the low-temperature spectra presented in Figure 2, since it precludes the presence of a 4090 cm^{-1} band without an accompanying band at ∼4125 cm^{-1} arising from H_2 in the secondary sites. Moreover, their scheme

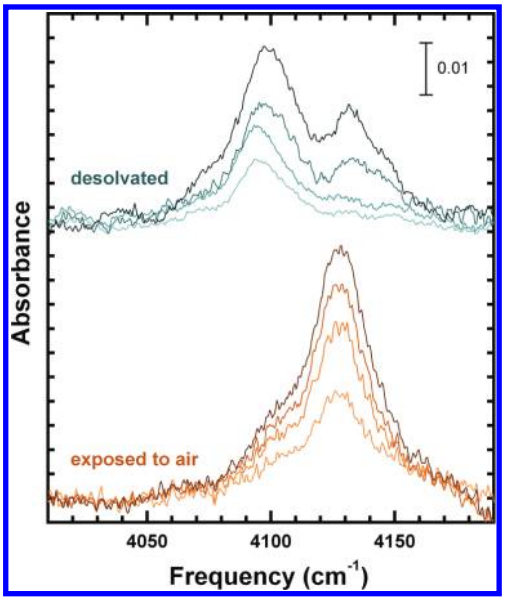

Figure 3. Concentration dependencies of *Q*-bands in the spectra of H_2 in desolvated Zn_2**L** (upper traces, blue/gray) and the same sample after exposure to ambient air for 5 min (lower traces, orange/brown). Spectra were acquired at 298 K for loading pressures of 25, 40, 50, and 100 bar (bottom to top of each grouping).

predicts the 4090 cm^{-1} band would reach a maximum intensity at concentrations above 2 H_2/M as molecular pairs are formed. The main data cited by Chabal and co-workers to justify their band assignments are spectra acquired at room temperature with high pressures of H_2.

To resolve this disagreement, we attempted to reproduce the experiments performed by the Chabal group using Zn_2**L** that had been carefully desolvated at 200 °C and handled under an inert atmosphere. Spectra collected at room temperature (Figure 3, upper traces) show that at the smallest H_2 loading pressure (25 bar) a single broad band is observed, centered at 4095 cm^{-1}. Increasing the H_2 pressure to 40 bar causes the intensity of the band to increase, but produces no other significant changes. Further H_2 loading (50 bar) leads to the appearance of a new band at 4135 cm^{-1}. The intensity of this band increases significantly at the largest loading pressure of 100 bar. These results are consistent extrapolations of our low-temperature data. The open metal coordination site is still the first populated; however, its enthalpic advantage is less dominant at room temperature. Entropic effects are more apparent, in that the secondary sites begin to be occupied before the primary site is completely filled. The larger widths of the bands at room temperature make it impossible to distinguish the bands of the secondary sites from each other, and most likely the band at 4135 cm^{-1} arises from H_2 in multiple environments. Notably, these spectra are different from those reported by Chabal and co-workers for (ostensibly) the same material under the same conditions.

It was not until we deliberately exposed our Zn_2**L** sample to air for 5 min, evacuated it at room temperature, and then repeated the H_2 loading experiment that we acquired spectra comparable to those in ref 35. At each pressure, the spectra are dominated by a single broad band centered at 4126 cm^{-1} (see Figure 3, lower traces). During preparation of this manuscript, a second paper was published by Chabal and co-workers with analogous findings for Co_2**L**.[44] We thus repeated our analyses with Co_2**L** both before

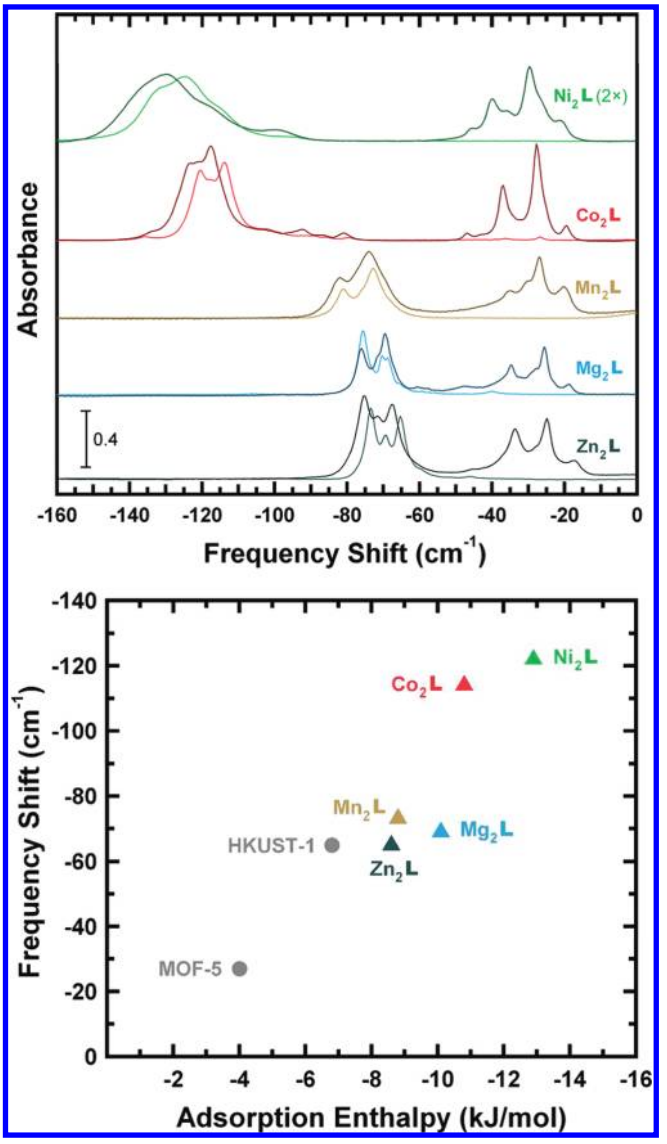

Figure 4. Upper plot: the purely vibrational *Q*-region of the spectra of H_2 in M_2**L** with the frequency scale referenced to that of the gas phase *Q*(0) value, 4161 cm^{-1}. Spectra correspond to those in Figure 1. Lower plot: positive correlation between the frequency shifts of the lowest concentration *Q*(0) band and reported isosteric enthalpies of adsorption at zero surface coverage (data from refs 20, 30, 31, 36, 45).

and after air-exposure and observed an even more pronounced effect, with the dominant room-temperature band changing from 4050 cm^{-1} in a pristine sample to 4125 cm^{-1} after exposing the sample to air (see Figure S10). Again, the spectra from the contaminated sample are similar to those published in ref 44.

We have observed this sensitivity to atmospheric moisture in many different MOF samples. Whenever the sample is exposed to air the intensities of the bands associated with the primary sites are diminished to the point where secondary site bands dominate the spectra. It is sensible that the primary site, being the most reactive, is the one most affected by contaminants. On the basis of the relative area of the two set of spectra in Figure 3 it appears that contamination of the primary site also increases the intensity of the bands associated with the secondary sites. This is most likely due to an increase in the induced dipole moment via water···H_2 interactions.

Table 1. Frequencies of the Fundamental Vibrational Mode *Q*(0) of Molecular Hydrogen Isotopologues at the Primary Adsorption Site of M_2L, Along with the Frequency Shift Relative to Gas Phase, Percentage Frequency Shift, and Frequency Shift of the Overtone Mode

gas	$\nu_{1\leftarrow0}$ (cm^{-1})	$\Delta\nu_{1\leftarrow0}$ (cm^{-1})	$\Delta\nu_{1\leftarrow0}/\nu_{1\leftarrow0}$ (%)	$\Delta\nu_{2\leftarrow0}/2$ (cm^{-1})
		Mg_2**L**		
H_2	4092	−69	−1.66	−68.5
HD	3570	−61	−1.68	−63.0
D_2	2940	−52	−1.74	−53.5
		Mn_2**L**		
H_2	4088	−73	−1.75	−74.5
HD	3566	−65	−1.79	−67.5
D_2	2936	−56	−1.87	−58.0
		Co_2**L**		
H_2	4047	−114	−2.74	*a*
HD	3529	−102	−2.81	−108
D_2	2904	−88	−2.94	−92.0
		Ni_2**L**		
H_2	4036	−125	−3.00	−134
HD	3518	−113	−3.11	−118
D_2	2889	−103	−3.44	*a*
		Zn_2**L**		
H_2	4096	−65	−1.56	−66.5
HD	3518	−58	−1.60	−61.0
D_2	2889	−50	−1.67	−52.5

[a] Unobserved due to low signal-to-noise.

Correlations Between the Vibrational Frequency Shift and Adsorption Enthalpy. Figure 4 shows the purely vibrational *Q*-region of the spectrum for adsorbed H_2 in M_2**L** materials, with frequencies shown as red shifts from the vibrational mode *Q*(0) of gaseous H_2, 4161 cm^{-1}. Our observed frequencies are summarized in Table 1 and are consistent with the findings of other groups.[11,24,35,44] At low concentration, where only the primary site is filled, the red shift of the *Q*(0) band almost doubles upon substitution of Ni for Zn in the structure. The bands from Ni_2**L** and Co_2**L** are significantly more red-shifted than the other members of the series. In contrast, the bands associated with the secondary sites exhibit a much smaller variation. This reduced dependence on the metal cation is to be expected, since the secondary sites are located farther from the metal ion (>4.8 Å compared to 2.6 Å).[34] The slightly lower frequency bands associated with each type of site arise from *ortho*-H_2. The reason for two or more such bands is the anisotropic nature of the interaction potential, which leads to a lifting of the degeneracy of the $J = 1$ rotational levels.[34]

Several groups have shown that the first H_2 bands to appear are those with the largest vibrational red shifts and that there is a correlation between large red shifts and large adsorption enthalpies.[11,24,28] This was disputed, however, in a recent paper

wherein room temperature spectra from a diverse set of MOFs displayed only minor variations.[46] The shortcoming of room temperature spectra is their tendency to exhibit broad features resulting from overlapping bands of H_2 in many different sites (vide supra). In contrast, low temperature spectra acquired with small concentrations of H_2 contain bands corresponding to the most favorable site and therefore can be directly compared with isosteric enthalpies of adsorption (in the limit of zero coverage) measured independently. Data compiled from this study and reports from the literature are shown in Figure 4 (bottom). While a positive correlation between binding energy and frequency shift is not always obeyed, the overall the trend is clear: IR band red shifts increase with adsorption enthalpy. The largest uncertainties in these data correspond to the isosteric enthalpies of adsorption, which show a variation on the order of 1 kJ/mol among reports from different groups.[45,47]

Evidence for Intermolecular $H_2\cdots H_2$ Interactions. From inspection of the spectra in Figure 1 it is clear that bands assigned to H_2 at the primary site display small changes with increasing H_2 concentration. This effect is most pronounced for the $S(0)$ band in the region 4300−4380 cm^{-1}. For each of the materials we observe a red shift of approximately 6 cm^{-1} as the concentration is increased from less than 0.1 H_2/M to greater than 3 H_2/M. Rather than a continuous change in frequency with concentration, each band is supplanted with a new band at the lower frequency and the transfer of intensity is continuous with increasing concentration. In the Q-region the frequency change is smaller, between 2 and 5 cm^{-1}, with the largest changes being observed for the Co and Ni materials.

Intermolecular interactions between the adsorbed H_2 are the probable origin of these band shifts. The fact that the spectral changes in the primary site bands are observed only for concentrations greater than 1 H_2/M points to interactions between molecules at the primary site with those at secondary sites. This interpretation is consistent with the neutron diffraction models,[34] which show the distance between primary sites is large (5.3 Å), while the distance between adjacent primary and secondary sites is less than 2.9 Å, comparable to the kinetic diameter of H_2. These weakly attractive interactions increase the total binding energy and alter the anisotropy of the orientational potential energy surface of each site. The additional anisotropy manifests itself through changes in the rotational J sublevels and the observed large shifts of the S bands.

An additional result of increasing the H_2 concentration is the substantial broadening of the center-of-mass translational modes in the region 4200−4300 cm^{-1}. This is most recognizable in Figure 2, where the full-width-at-half-maximum of the translational band in the largest concentration spectrum (top) is more than double that in the smaller concentration spectra. This behavior reflects the changes in the center-of-mass potential energy surface at the primary site. The additional anisotropy resulting from interactions with H_2 on the secondary sites increases the spread of the different translational modes, broadening the observed band.

We are aware of only one theoretical approach aimed at modeling the spectral perturbation due to $H_2\cdots H_2$ interactions in a porous material. The paper by the Chabal group, discussed above, describes vdW-DFT calculations that predict concentration-dependent Q-band frequency shifts of 21 and 16 cm^{-1} for Zn_2**L** and Mg_2**L**, respectively.[35] These are significantly larger than our experimentally observed shifts of 2.0 and 1.6 cm^{-1} for the primary site bands of the respective systems.

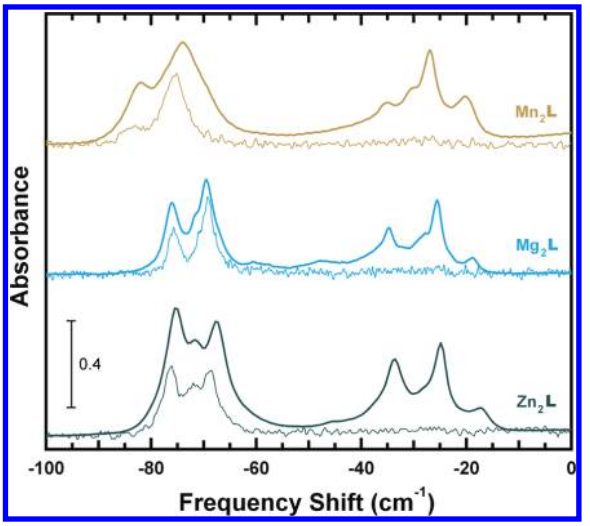

Figure 5. Fundamental (bold traces) and overtone (fine traces) portions of the same spectrum for H_2 in each of Mn_2**L**, Mg_2**L**, and Zn_2**L** loaded with 2 H_2/M at 35 K. The frequency shifts of the overtone spectra were divided by 2, and their intensities are magnified by a factor of 4 for comparison with the fundamental bands.

Isotope Effects. In his seminal paper, Buckingham showed that for a diatomic molecule with rotational constant B_e and harmonic frequency ω_e the ratio of B_e/ω_e^2 is unaffected by isotopic substitution.[48] Thus, to second-order perturbation the fractional vibrational shift of different hydrogen isotopologues should be equal, i.e., $\Delta\nu/\nu_{free}$ = constant.

To examine the validity of the Buckingham model for describing the dynamics of H_2 isotopologues in M_2**L**, we acquired low temperature spectra for each of the materials exposed to HD and D_2. The results, summarized in Table 1 and Figure S11, reveal only small deviations from the Buckingham prediction with a systematic increase in the fractional frequency shift with increasing molecular mass. The excellent consistency among the different isotopologues removes any possibility that the highly red-shifted bands arise from the pairing mechanism proposed by ref 35, since they accept that pairs should not be formed with D_2. The minor systematic increase in the fractional frequency shift may be explained by vibrational−translational coupling, in which the greater D_2 mass leads to a smaller translational zero-point energy and a deeper residence within the confining potential energy well. The heavier isotopologues experience slightly larger adsorption enthalpies and consequently larger fractional red shifts. This enhanced binding has been observed in the adsorption isotherms for other MOFs,[31,49] and it has been speculated that it could be employed in separation technology.[50−51]

Overtone Bands. In the absence of increased anharmonicity of an adsorbed H_2, the Buckingham model also predicts the vibrational shift of the overtone mode should be double that of the fundamental, $\Delta\nu(2\leftarrow0) = 2\,\Delta\nu(1\leftarrow0)$.[48] Discrepancies from this behavior can be used to assess the degree to which surface interactions mix the vibrational energy states of an adsorbed molecule. Despite the value of this information, overtone bands are rarely reported for adsorbed H_2,[54−56] and to our knowledge they have not been discussed in the literature surrounding MOFs. Detecting these weak transitions may be quite challenging; since ab initio calculations predict overtone intensities to be only a few percent of those of the corresponding fundamentals.[57,58] An advantage of the diffuse reflectance optical geometry used here is

the amplification of weak bands. This has afforded us the opportunity to observe and compare H_2 overtones in the ~8000 cm^{-1} region.

To directly compare the red shifts of the overtone bands with those of the corresponding fundamentals of H_2 in the different materials, we have prepared the reduced plots shown in Figure 5. Only data for the Mg_2**L**, Mn_2**L**, and Zn_2**L** are presented, as the overtone bands from H_2 in Ni_2**L** were too weak to be observed and Co_2**L** has a strong framework absorption in this region. The frequency shifts, summarized in Table 1, are in good agreement with predictions from the Buckingham model, indicating that any induced anharmonicity is minor. The overtone modes of H_2 at the primary site are remarkably intense, with integrated areas ranging from 10% to 20% of that of the fundamental. This is significantly higher than the 3% ratio observed for H_2 in zeolites using the transmission geometry.[54] Interestingly, we did not detect overtone bands arising from H_2 at any secondary sites. While overtone enhancement appears to be limited to the primary sites, it occurs for all of the M_2**L** materials, and it is even stronger for the HD and D_2 isotopologues. We are presently working on a theoretical model to explain this large increase in the overtone intensity.

5. SUMMARY

We have determined that for adsorbed hydrogen within the M_2**L** series the most highly red-shifted vibrational features arise from isolated H_2 molecules at the primary site associated with the coordinatively unsaturated metals and not from a proposed $H_2\cdots H_2$ pairing mechanism.[35] We have presented further evidence that the magnitudes of these red shifts correlate with the adsorption enthalpies of the sites. As expected, the secondary sites, which become occupied only after the primary site is filled, give rise to IR features that are largely insensitive to metal substitution. Frequency shifts revealed by isotopologue substitution spectra (HD and D_2) and overtone spectra show good agreement with the Buckingham model predictions.[48] From this we can conclude that interactions with the primary site cause only minor changes to the H_2 anharmonicity. This is an important consideration for accurately modeling the interactions at each adsorption site. Finally, we observed small, but distinct, changes in the primary site IR bands after population of the secondary sites. We attribute this behavior to weak $H_2\cdots H_2$ interactions; however, the magnitude of the effect is much smaller than recently published theoretical predictions.[35] We hope this work resolves some of the uncertainties surrounding this system and inspires the development of an improved theoretical model to describe H_2 adsorption in future materials, be they established materials with known structures or hypothetical candidates.

■ ASSOCIATED CONTENT

Supporting Information. Powder X-ray diffraction patterns of the samples; results of thermogravimetric analyses; mid-IR spectra of the desolvated samples; table of characteristic IR absorption frequencies for each sample; mid-IR spectra of rehydrated Zn_2**L**; hydrogen adsorption isotherms; diffuse reflectance IR spectra of H_2 in Co_2**L** at room temperature; diffuse reflectance IR spectra of H_2, HD, and D_2 in the samples. This material is available free of charge via the Internet at http://pubs.acs.org.

■ AUTHOR INFORMATION

Corresponding Author
stephen.fitzgerald@oberlin.edu; jesse.rowsell@oberlin.edu

■ ACKNOWLEDGMENT

This work was partially funded by the American Chemical Society Petroleum Research Fund and the Oberlin Department of Chemistry and Biochemistry.

■ REFERENCES

(1) Ferey, G.; Mellot-Draznieks, C.; Serre, C.; Millange, F.; Dutour, J.; Surble, S.; Margiolaki, I. *Science* **2005**, *309*, 2040.
(2) Dinca, M.; Dailly, A.; Liu, Y.; Brown, C. M.; Neumann, D. A.; Long, J. R. *J. Am. Chem. Soc.* **2006**, *128*, 16876.
(3) Furukawa, H.; Miller, M. A.; Yaghi, O. M. *J. Mater. Chem.* **2007**, *17*, 3197.
(4) Cavka, J. H.; Jakobsen, S.; Olsbye, U.; Guillou, N.; Lamberti, C.; Bordiga, S.; Lillerud, K. P. *J. Am. Chem. Soc.* **2008**, *130*, 13850.
(5) Ma, S. Q.; Eckert, J.; Forster, P. M.; Yoon, J. W.; Hwang, Y. K.; Chang, J. S.; Collier, C. D.; Parise, J. B.; Zhou, H. C. *J. Am. Chem. Soc.* **2008**, *130*, 15896.
(6) Lin, X.; Telepeni, I.; Blake, A. J.; Dailly, A.; Brown, C. M.; Simmons, J. M.; Zoppi, M.; Walker, G. S.; Thomas, K. M.; Mays, T. J.; Hubberstey, P.; Champness, N. R.; Schroder, M. *J. Am. Chem. Soc.* **2009**, *131*, 2159.
(7) Koh, K.; Wong-Foy, A. G.; Matzger, A. J. *J. Am. Chem. Soc.* **2009**, *131*, 4184.
(8) Sumida, K.; Hill, M. R.; Horike, S.; Dailly, A.; Long, J. R. *J. Am. Chem. Soc.* **2009**, *131*, 15120.
(9) Furukawa, H.; Ko, N.; Go, Y. B.; Aratani, N.; Choi, S. B.; Choi, E.; Yazaydin, A. O.; Snurr, R. Q.; O'Keeffe, M.; Kim, J.; Yaghi, O. M. *Science* **2010**, *329*, 424.
(10) Bhatia, S. K.; Myers, A. L. *Langmuir* **2006**, *22*, 1688.
(11) Areán, C. O.; Chavan, S.; Cabello, C. P.; Garrone, E.; Palomino, G. T. *ChemPhysChem* **2010**, *11*, 3237.
(12) Bae, Y. S.; Snurr, R. Q. *Microporous Mesoporous Mater.* **2010**, *132*, 300.
(13) Stephanie-Victoire, F.; Goulay, A. M.; de Lara, E. C. *Langmuir* **1998**, *14*, 7255.
(14) Dinca, M.; Long, J. R. *Angew. Chem., Int. Ed.* **2008**, *47*, 6766.
(15) Zavorotynska, O.; Vitillo, J. G.; Spoto, G.; Zecchina, A. *Int. J. Hydrogen Energy* **2011**, *36*, 7944.
(16) Rosi, N. L.; Kim, J.; Eddaoudi, M.; Chen, B. L.; O'Keeffe, M.; Yaghi, O. M. *J. Am. Chem. Soc.* **2005**, *127*, 1504.
(17) Dietzel, P. D. C.; Johnsen, R. E.; Blom, R.; Fjellvag, H. *Chem.—Eur. J.* **2008**, *14*, 2389.
(18) Caskey, S. R.; Wong-Foy, A. G.; Matzger, A. J. *J. Am. Chem. Soc.* **2008**, *130*, 10870.
(19) Dietzel, P. D. C.; Blom, R.; Fjellvag, H. *Eur. J. Inorg. Chem.* **2008**, 3624.
(20) Zhou, W.; Wu, H.; Yildirim, T. *J. Am. Chem. Soc.* **2008**, *130*, 15268.
(21) Bhattacharjee, S.; Choi, J. S.; Yang, S. T.; Choi, S. B.; Kim, J.; Ahn, W. S. *J. Nanosci. Nanotechnol.* **2010**, *10*, 135.
(22) Dietzel, P. D. C.; Morita, Y.; Blom, R.; Fjellvag, H. *Angew. Chem., Int. Ed.* **2005**, *44*, 6354.
(23) Dietzel, P. D. C.; Panella, B.; Hirscher, M.; Blom, R.; Fjellvag, H. *Chem. Commun.* **2006**, 959.
(24) Vitillo, J. G.; Regli, L.; Chavan, S.; Ricchiardi, G.; Spoto, G.; Dietzel, P. D. C.; Bordiga, S.; Zecchina, A. *J. Am. Chem. Soc.* **2008**, *130*, 8386.
(25) Kazansky, V. B.; Borovkov, V. Y.; Karge, H. G. *J. Chem. Soc., Faraday Trans.* **1997**, *93*, 1843.
(26) Kazansky, V. B.; Jentoft, F. C.; Karge, H. G. *J. Chem. Soc., Faraday Trans.* **1998**, *94*, 1347.
(27) Borovkov, V. Y.; Serykh, A. I.; Kazansky, V. B. *Kinet. Catal.* **2000**, *41*, 787.
(28) Bordiga, S.; Vitillo, J. G.; Ricchiardi, G.; Regli, L.; Cocina, D.; Zecchina, A.; Arstad, B.; Bjorgen, M.; Hafizovic, J.; Lillerud, K. P. *J. Phys. Chem. B* **2005**, *109*, 18237.
(29) FitzGerald, S. A.; Churchill, H. O. H.; Korngut, P. M.; Simmons, C. B.; Strangas, Y. E. *Phys. Rev. B* **2006**, *73*, 155409.

(30) Bordiga, S.; Regli, L.; Bonino, F.; Groppo, E.; Lamberti, C.; Xiao, B.; Wheatley, P. S.; Morris, R. E.; Zecchina, A. *Phys. Chem. Chem. Phys.* **2007**, *9*, 2676.
(31) FitzGerald, S. A.; Allen, K.; Landerman, P.; Hopkins, J.; Matters, J.; Myers, R.; Rowsell, J. L. C. *Phys. Rev. B* **2008**, *77*, 224301.
(32) Kong, L. Z.; Cooper, V. R.; Nijem, N.; Li, K. H.; Li, J.; Chabal, Y. J.; Langreth, D. C. *Phys. Rev. B* **2009**, *79*, 081407.
(33) FitzGerald, S. A.; Hopkins, J.; Burkholder, B.; Friedman, M.; Rowsell, J. L. C. *Phys. Rev. B* **2010**, *81*, 104305.
(34) Liu, Y.; Kabbour, H.; Brown, C. M.; Neumann, D. A.; Ahn, C. C. *Langmuir* **2008**, *24*, 4772.
(35) Nijem, N.; Veyan, J. F.; Kong, L. Z.; Wu, H. H.; Zhao, Y. G.; Li, J.; Langreth, D. C.; Chabal, Y. J. *J. Am. Chem. Soc.* **2010**, *132*, 14834.
(36) Rowsell, J. L. C.; Yaghi, O. M. *J. Am. Chem. Soc.* **2006**, *128*, 1304.
(37) FitzGerald, S. A.; Churchill, H. O. H.; Korngut, P. M.; Simmons, C. B.; Strangas, Y. E. *Rev. Sci. Instrum.* **2006**, *77*, 093110.
(38) Bragg, S. L.; Brault, J. W.; Smith, W. H. *Astrophys. J.* **1982**, *263*, 999.
(39) Herzberg, G. *Infrared and Raman Spectra*; D. Van Nostrand Company Inc.: New York, 1996.
(40) FitzGerald, S. A.; Forth, S.; Rinkoski, M. *Phys. Rev. B* **2002**, 65.
(41) Herman, R. M.; Lewis, J. C. *Phys. Rev. B* **2006**, *73*, 155408.
(42) Gush, H. P.; Hare, W. F.; Allen, E. J.; Welsh, H. L. *Can. J. Phys.* **1960**, *38*, 176.
(43) McKellar, A. R.; Clouter, M. J. *Can. J. Phys.* **1994**, *72*, 51.
(44) Nijem, N.; Kong, L. Z.; Zhao, Y. G.; Wu, H. H.; Li, J.; Langreth, D. C.; Chabal, Y. J. *J. Am. Chem. Soc.* **2011**, *133*, 4782.
(45) Murray, L. J.; Dinca, M.; Long, J. R. *Chem. Soc. Rev.* **2009**, *38*, 1294.
(46) Nijem, N.; Veyan, J. F.; Kong, L. Z.; Li, K. H.; Pramanik, S.; Zhao, Y. G.; Li, J.; Langreth, D.; Chabal, Y. J. *J. Am. Chem. Soc.* **2010**, *132*, 1654.
(47) Thomas, K. M. *Dalton Trans.* **2009**, 1487.
(48) Buckingham, D. A. *Trans. Faraday Soc.* **1960**, *56*, 753.
(49) Xiao, B.; Wheatley, P. S.; Zhao, X. B.; Fletcher, A. J.; Fox, S.; Rossi, A. G.; Megson, I. L.; Bordiga, S.; Regli, L.; Thomas, K. M.; Morris, R. E. *J. Am. Chem. Soc.* **2007**, *129*, 1203.
(50) Garberoglio, G.; DeKlavon, M. M.; Johnson, J. K. *J. Phys. Chem. B* **2006**, *110*, 1733.
(51) Chen, B.; Zhao, X.; Putkham, A.; Hong, K.; Lobkovsky, E. B.; Hurtado, E. J.; Fletcher, A. J.; Thomas, K. M. *J. Am. Chem. Soc.* **2008**, *130*, 6411.
(52) Wang, Y.; Bhatia, S. K. *Mol. Simul.* **2009**, *35*, 162.
(53) Nguyen, T. X.; Jobic, H.; Bhatia, S. K. *Phys. Rev. Lett.* **2010**, *105*, 085901.
(54) Forster, H.; Frede, W. *Infrared Phys.* **1984**, *24*, 151.
(55) Knippers, W.; Vanhelvoort, K.; Stolte, S. *Chem. Phys. Lett.* **1985**, *121*, 279.
(56) Bose, H.; Forster, H.; Frede, W. *Chem. Phys. Lett.* **1987**, *138*, 401.
(57) Karl, G.; Poll, J. D. *J. Chem. Phys.* **1967**, *46*, 2944.
(58) Schwartz, C.; Leroy, R. J. *J. Mol. Spectrosc.* **1987**, *121*, 420.